1-Picosecond InGaAs Photodetector for Operation at 1300-1600 nm

N00014-93-C-0134

Progress Report No. 2 for work done 9/15/93 - 11/15/93

During the past two months we have grown a number of new InGaAs structures and characterized them for sensitivity, speed, resistivity, and optical absorption. Based on our findings we have decided to shift emphasis away from further work on mismatched epilayers grown on either GaAs or InP. We have concentrated on two new approaches that promise to shorten carrier lifetime while maintaining high sensitivity, and resistivity.

The first approach involves growing a superlattice of low-temperature MBE InGaAs/InAlAs with post annealing, ie. InGaAs:As/InAlAs:As. (We use the follow convention: low-temperature gro vn but *without* post-annealing is referred to as LT-InGaAs/GaAs, low-temperature grown with annealing is referred to as InGaAs:As/InAlAs:As). In this structure, the InGaAs:As serves as an absorbing layer while the InAlAs:As as a trapping layer. The III-V materials group at Martin Marietta has grown these samples for us. We discuss our initial results in this report. The second approach, for which samples are now being grown, uses lattice-matched bulk (ie. no superlattice) InGaAs:As. Past work on InGaAs:As showed that the material had a picosecond carrier lifetime but low resistivity (~ 1 Ω-cm). We believe this is due to Fermi level pinning near the conduction band. We will attempt to remedy this problem by introducing a p-type dopant to compensate the lattice and restore the Fermi level to mid gap. This work will be carried out in collaboration with a new company known as Mellwood Labs, Inc. Mellwood Labs is a spin-off of Purdue University founded by Mike Melloch and Jerry Woodall, who are recognized experts in the field of non-stoichiometric semiconductors.

Polycrystalline LT:InGaAs We began our Phase I program studying low-temperature MBE-grown InGaAs with no post annealing (LT-InGaAs), and lattice mismatched on GaAs. At the time, this was the only means for simultaneously achieving picosecond carrier lifetimes and high resistivity in InGaAs.

In our previous report we showed the absorption curve for low-temperature grown $In_{0.35}Ga_{0.65}As$ epilayer on GaAs. We referred to this epilayer as highly strained. In fact, for layer thicknesses greater than 100 Å this large a lattice mismatch (from $In_{0.35}Ga_{0.65}As$ to GaAs, or

~2.5% strain) can only be of polycrystalline morphology, as evidenced by the blurred absorption edge on the absorption curve. The relatively low absorption coefficient of $5x10^3$ cm^{-1} at 1300 nm translates into a 1/e penetration depth of 2 micrometers. To fully detect all photons would require us to space the interdigitated fingers, that form the MSM detector, 2 micrometers apart. For a semiconductor with a carrier lifetime on the order of 1 picosecond, this finger spacing will yield a responsivity less than 0.05 A/W, even for high mobility material.

Unlike single-crystal InGaAs:As, where fast lifetime is obtained from arsenic precipitates that behave as buried Schottky barriers, polycrystalline semiconductors derive their speed from material defects. Along with excess arsenic, the presence of inclusions, point defects, and dislocations serve to reduce the carrier lifetime to a few picoseconds. In fact, it is not clear what contribution the excess arsenic plays in reducing the carrier lifetime in polycrystalline LT-InGaAs. If we post annealed polycrystalline LT-InGaAs to form arsenic precipitates we would not see the carrier lifetime drop nor the resistivity rise, as is the case with single crystal LT-InGaAs after annealing. Instead, the opposite occurs, the carrier lifetime increases and the resistivity drops. Annealing this material causes the polycrystalline clusters to grow larger and eliminates the interfacial defects and damage that create the desired properties. The problem with defects is that they give rise to large density of states and thermally-ionized carriers which reduces the sheet resistance by more than one order of magnitude. Material defects also lower the mobility by impeding the propagation of photocarriers.

By comparison, single-crystal InGaAs:As is comprised of defect-free InGaAs and arsenic precipitates equally space with a density of 10^{15}-10^{17} cm^{-3}. The Schottky field from adjacent precipitates overlap to provide highly-depleted region that has mobility exceeding 500 $cm^2/V \cdot s$. For polycrystalline InGaAs the mobility is $\leq$ 10 $cm^2/V \cdot s$. Low mobility and low resistivity, coupled with a low absorption coefficient, have yielded an InGaAs detector with a responsivity of 0.001 A/W and dark current of 1 mA. A 200-fold increase in responsivity and 10^6-fold increase in dark current would be needed for this device to be useful. In addition to its poor optoelectronic performance, lattice mismatched $In_{0.35}Ga_{0.65}As$ on GaAs has a coarse, sand paper-like surface, making it difficult for microfabrication. For these reasons we have decided to redirect our study to techniques that use only single-crystal InGaAs:As.

High-Resistivity InGaAs:As Lattice-matched LT-$In_{0.53}Ga_{0.47}As$ and $In_{0.53}Ga_{0.47}As$:As grown on InP both have a resistivity of ~ 1 Ω-cm. In contrast, the resistivity for GaAs:As is > 10^7 Ω-cm. To help us understand the effect indium has on resistivity we have grown a set of three lattice-matched samples for measuring sheet resistance. Figure 1 shows a curve of sheet resistance

vs. indium concentration for the three samples. The three solid points represent sheet resistance values for lattice-matched GaAs:As grown on GaAs, $In_{0.35}Al_{0.65}As$:As grown on a GaAs-based buffer layer graded from $In_{0.0}Al_{1.0}As$ to $In_{0.35}Al_{0.65}As$, and $In_{0.53}Al_{0.47}As$:As grown on InP. For reference we also show the sheet resistance for polycrystalline LT-$In_{0.35}Al_{0.65}As$. We see that the sheet resistance drops by 8 orders of magnitude from $3x10^{11}$ Ω/square to $5x10^{3}$ Ω/square as the indium concentration is increased from 0-53%. We have taken one of these samples, $In_{0.35}Al_{0.65}As$:As (sample M1331), and measured its transient optical reflectivity. Figure 2 shows a family of four traces taken for increasing post anneal temperatures. Despite its low sheet resistance, we see that $In_{0.35}Al_{0.65}As$:As has a carrier lifetime that is < 10 picoseconds. It is interesting to note that the annealing process has little effect on the carrier lifetime, with the as-grown and annealed lifetimes differing by at most a factor of two. The sheet resistance, on the other hand, was found to increase by 20-fold after annealing.

A possible explanation for the low resistivity of InGaAs is offered in Fig. 3. Shown is a set of four simplified band diagrams for GaAs and InGaAs. The first diagram depicts the energy positions of the conduction and valence band edges, as well as the relative position of the Fermi level for unintentionally doped GaAs. We note that the Fermi level is at the midgap, 0.7 eV above the valence band.

Arsenic precipitates are a deep-level traps that behave like dual deep donors and deep acceptors to render the material semi-insulating. In the second diagram we show LT-GaAs with upwards of 10^{19} cm^{-3} arsenic antisite defects being pinned 0.9 eV above the valence band. After annealing the arsenic antisites aggregate into Schottky precipitates with a pinned barrier height of 0.7 eV. The difference in sheet resistance for these two states is significant, 10^{3} Ω/square vs. 10^{11} Ω/square for the unanneal and post annealed, respectively. The third diagram shows the band structure for $In_{0.35}Ga_{0.65}As$:As. The Fermi level is no longer at midgap but pinned closer to the conduction band. The semiconductor in this case is n-type which yields considerably higher sheet resistance. The last diagram shows the band structure for $In_{0.53}Ga_{0.46}As$:As. The Fermi level is pinned just below the conduction band, resulting in an extremely high concentration of thermally-ionized carriers.

We now describe two approaches we are taking to attempt to increase the resistivity of InGaAs:As. The first approach separates the functions of absorption and trapping in InGaAs by utilizing a superlattice structure formed of InGaAs:As and InAlAs:As.

$In_{0.53}Ga_{0.47}As$:As / $In_{0.52}Al_{0.48}As$:As Superlattice We have begun work on a new concept that utilizes the high resistivity and fast carrier lifetime of InAlAs:As combined in a superlattice with InGaAs:As to achieve the above mentioned properties. $In_{0.52}Al_{0.48}As$ is lattice matched to InP and $In_{0.53}Ga_{0.46}As$. It has a bandgap close to that of GaAs, making it of little use for long-wavelength detectors on its own. If we grow alternate layers of absorbing InGaAs and InAlAs we should be able to both absorb the long-wavelength optical signal and trap the carriers. We have grown $In_{0.53}Ga_{0.47}As$:As / $In_{0.52}Al_{0.48}As$:As superlattices on InP with 200-Å layer thicknesses to demonstrate the concept. We chose the 200 Å thickness to be close to the spacing of the precipitates normally found in GaAs:As. We also grew a bulk layer of $In_{0.52}Al_{0.48}As$:As to measure its optoelectronic properties separately. Figure 4 shows the absorption curve for $In_{0.52}Al_{0.48}As$:As, along with the layer profile.

Figure 5 shows the transient reflectivity for this material and for a sample grown under normal temperature. The sheet resistance for the $In_{0.52}Al_{0.48}As$:As sample is 10^9 Ω/square. Figure 6 shows the absorption curve for the superlattice structure, along with its layer profile. The structure was grown on semi-insulating InP starting with a 1000-Å layer of $In_{0.52}Al_{0.48}As$ grown at normal stoichiometric temperature (520° C) and followed by a second 1000-Å layer of $In_{0.52}Al_{0.48}As$ grown as the temperature dropped from 520° C to 245° C. The superlattice was then grown with alternating layers of 200-Å thickness $In_{0.53}Ga_{0.46}As$ and $In_{0.52}Al_{0.48}As$, and capped with a 200-Å layer of $In_{0.53}Ga_{0.46}As$. The sample was then post annealed at 470° C for 10 minutes in an arsenic overpressure. The action of post annealing causes excess arsenic in the InGaAs layer to be gettered into the adjacent InAlAs layers, where is aggregates into precipitates of similar size and spacing as found in bulk grown InAlAs:As. The 200 Å thickness assures that the InGaAs will be fully depleted. Going larger than 200 Å for the InGaAs thickness might reduce the effect of the Schottky precipitates. Going thinner of course reduces the effective absorption. We also selected 200 Å for the InAlAs layer, which simplified the growth procedure and assured a sufficiently thick region to trap carriers.

The ripples that appear on the absorption curve of Fig. 6 correspond to the periodicity for multiple quantum wells of 200 Å spacing. We expect to see an absorption edge approximately midway between the absorption edge for $In_{0.52}Al_{0.48}As$ (825 nm) and $In_{0.53}Ga_{0.47}As$ (1550 nm), or ~1188 nm. It is difficult to discern from the surrounding features whether such an edge exist. We measured the sheet resistance for this material and found it to be 10^6 Ω/square, 500-fold improvement over bulk $In_{0.53}Ga_{0.46}As$:As (ref. to Fig. 1).

The dynamics for charge transport go as follows. Light is absorbed in the InGaAs layers creating electrons and holes. In the presence of a moderate electric field (10^3 V/cm) applied in the plane of the layers the photogenerated carriers are accelerated to sufficiently high energy to overcome the barrier potential and transfer into the wide bandgap InAlAs layers. Given the mobility for InGaAs and the 200-Å layer thickness, real space transfer should take 2-5 picoseconds. Once in the arsenic-rich InAlAs:As layers the carries are trapped within a few picoseconds. The presence of the electric field is important to accelerate the carriers and affect the thermionic emission process. If the field is perpendicular to the layers the carriers will accumulate at the interface and will be slow to tunnel through the interface. If sufficiently large light levels are absorbed in both the InGaAs and InAlAs, the 0.25-eV barrier will taper off via band bending to allow carriers to move more freely through the interface, even with no field applied.

This latter case was the set of conditions used to initially study charge transport in our samples. Figure 7 shows the transient reflectivity for the superlattice with a laser operating at 800 nm was used to produce electron-hole pairs. In this experiment carriers are generated both in the $In_{0.53}Ga_{0.47}As$:As and $In_{0.52}Al_{0.48}As$:As. The reflectivity shows that the material is indeed as fast as bulk $In_{0.52}Al_{0.48}As$:As. Time-resolved photoconductive measurements, with the light selectively absorbed by the InGaAs layers, are now needed to determine the true carrier lifetime for this material. These initial results are nevertheless encouraging.

$In_{0.53}Ga_{0.46}As$:As Compensated with p-Type Dopants: We had shown in Fig. 3 the effect arsenic had on the position of the Fermi level in InGaAs systems. As the molar fraction of indium is increased, the arsenic-rich InGaAs becomes more n-type and more conducting. Post annealing helps to restore the Fermi level to midgap, but only by reducing the overall arsenic level. As with all semiconductors, InGaAs moves to restore equilibrium as it is heated. For InGaAs:As, this means purging arsenic until the system is fully compensated, that is, until all arsenic is removed. The alternative technique, and the one now being explored, is to add a p-dopant, beryllium, so that InGaAs can be compensated without removing the arsenic. The precise amount of beryllium is not critical. The system will only purge the surplus dopant as it move towards self compensation. Samples of p-doped $In_{0.20}Ga_{0.80}As$ are now being grown and will be tested using a picosecond laser operating and 1064 nm.

Figure Captions

Fig. 1 Sheet resistance for post-annealed, lattice matched GaAs:As, $In_{0.35}Ga_{0.65}As$:As, $In_{0.53}Ga_{0.47}As$:As. The sheet resistance for polycrystalline LT-$In_{0.35}Ga_{0.65}As$ is also shown. The minimum acceptable values for sheet resistance for detector areas of 50x50 μm^2 and 8x8 μm^2 are shown and correspond to photoconductive dark current of ~ 1nA.

Fig. 2 Time-resolved all-optical transient reflectivity for $In_{0.35}Ga_{0.65}As$ pumped and probed with a 100-fs laser operating at 800 nm. The unannealed sample has a carrier lifetime of 14 ps (1/e), compared to 7 ps for the three post-annealed samples.

Fig. 3 Band diagrams for GaAs and InGaAs. After post annealing, the Fermi level for arsenic-rich GaAs returns to midgap. The presence of excess arsenic in InGaAs causes the Fermi level to move away from midgap and closer to the conduction band as the molar fraction of indium is increased.

Fig. 4 Spectraphotometer scan of bulk $In_{0.52}Ga_{0.48}As$ (shown in insert). The traces are the same except for the Y-axis scale. Absorption (ABS) is plotted in OD. The relation between the measured absorption and the absorption coefficient, α is: $\alpha[cm^{-1}] = -(1/T[cm])\ ln\ (10^{-ABS[OD]})$, where T is the epilayer's thickness. The bandedge for $In_{0.52}Ga_{0.48}As$ lies *above* that of the InP substrate, implying these curves are only measuring the absorption of the InP. We have included them for baseline comparison to the absorption curve in Fig. 6.

Fig. 5 Transient reflectivity of $In_{0.52}Ga_{0.48}As$, grown under normal stoichiometric conditions and of $In_{0.52}Ga_{0.48}As$:As. We believe the long undershoot found with the $In_{0.52}Ga_{0.48}As$:As curve is an artifact of the measurement technique. Picosecond photoconductive measurements on samples displaying an undershoot from transient reflectivity indicate no such tail in the photocurrent exist. Perhaps it is related to the deep-level traps.

Fig. 6 Spectraphotometer scan of $In_{0.53}Ga_{0.47}As$:As/$In_{0.52}Al_{0.48}As$:As superlattice (shown in insert). The ripples on the curve are due to the periodicity of the superlattice.

Fig. 7 Transient reflectivity of the $In_{0.53}Ga_{0.47}As$:As/$In_{0.52}Al_{0.48}As$:As superlattice. The measurement was made with both the pump and probe light being above the bandgap for the $In_{0.52}Al_{0.48}As$:As. Hence, carriers were photogenerated in both layers. Despite the suboptimal laser wavelengths, we see that the superlattice has a effective carrier lifetime of 8 picoseconds (1/e). The carrier lifetime of unintentionally-doped $In_{0.53}Ga_{0.47}As$ is several hundred picoseconds.

Sheet Resistance for Lattice-Matched $In_xGa_{1-x}As$:As

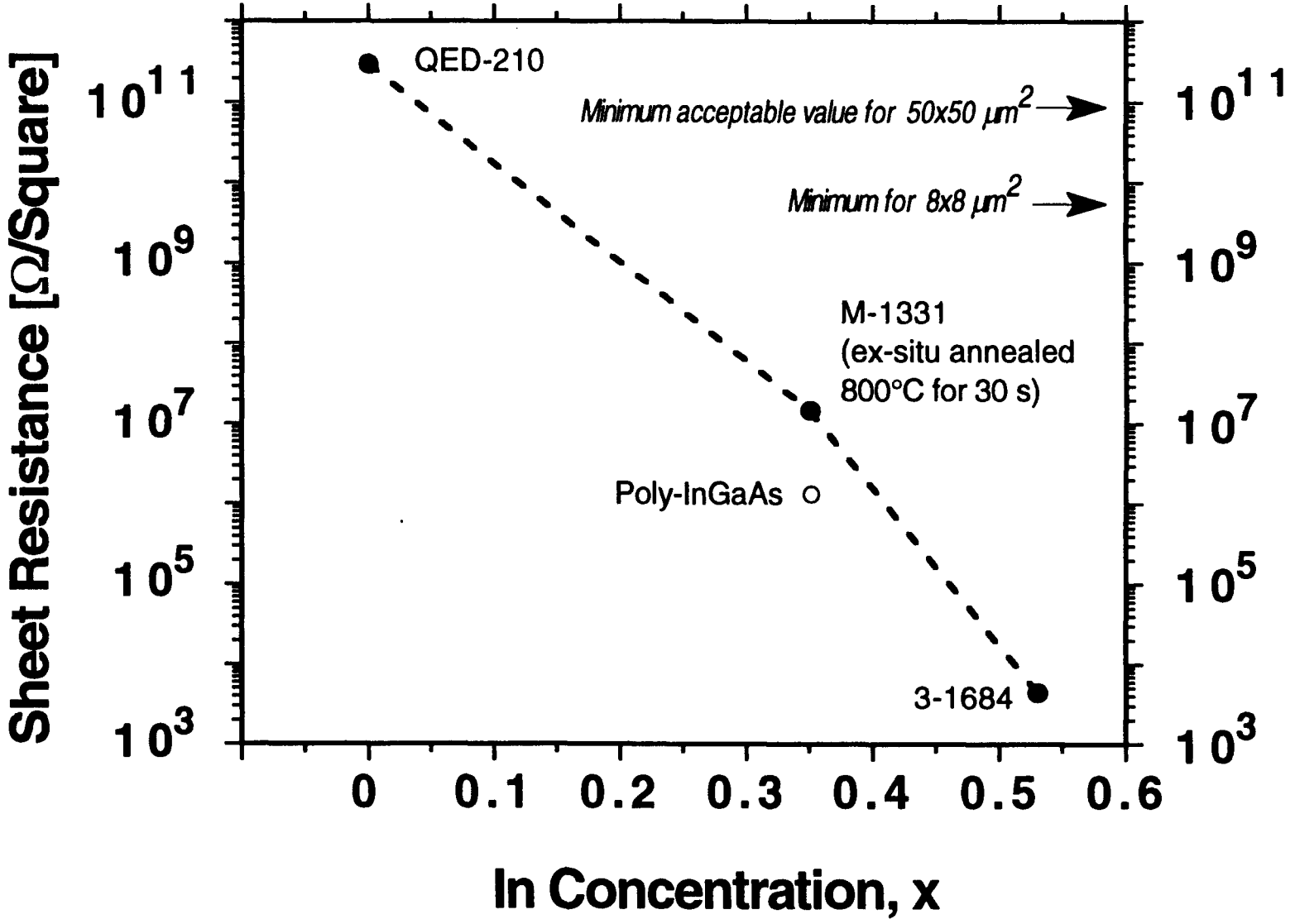

Fig. 1

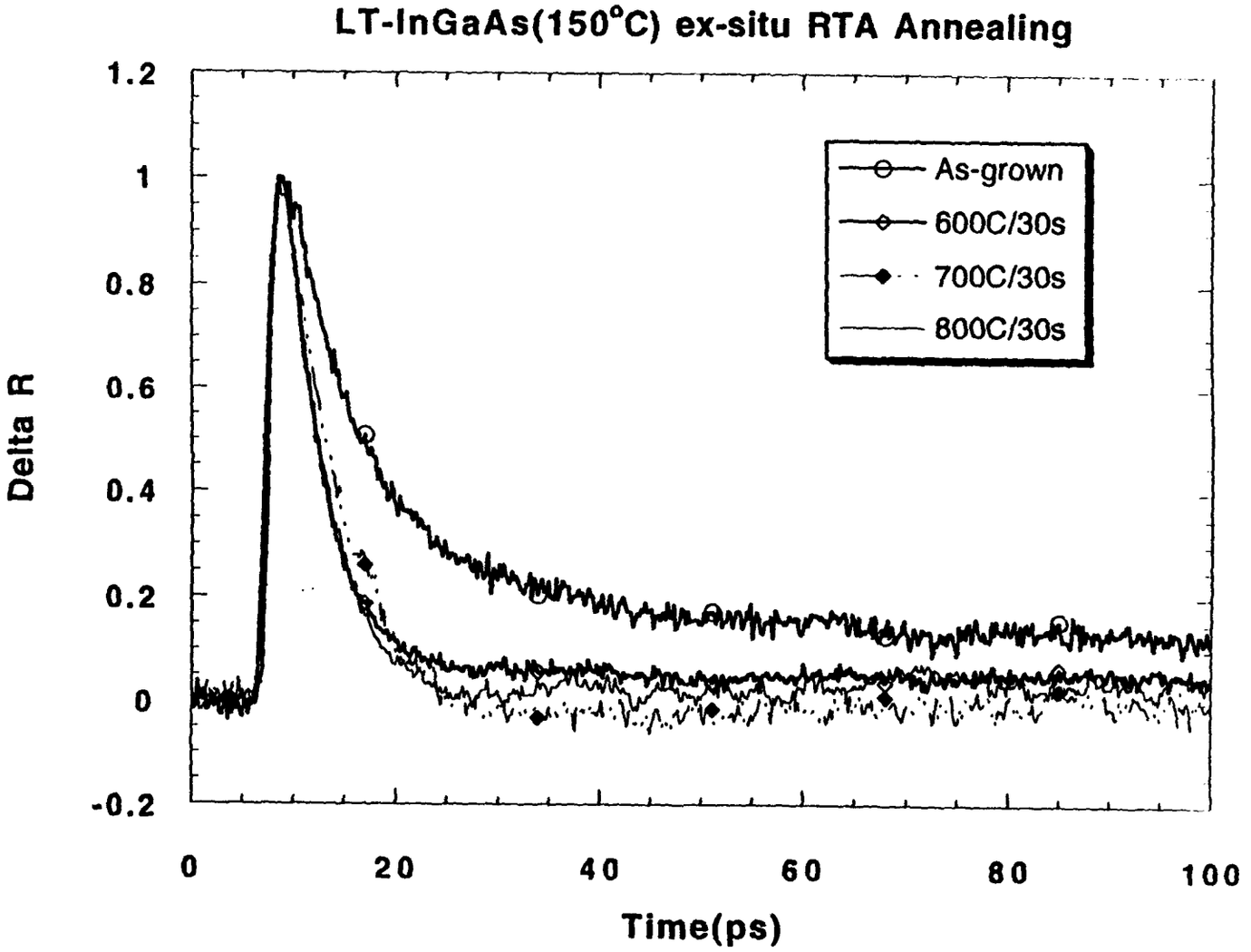
LT-InGaAs(150°C) ex-situ RTA Annealing
Delta R
1.2
1
0.8
0.6
0.4
0.2
0
-0.2
0
20
40
60
80
100
Time(ps)
As-grown
600C/30s
700C/30s
800C/30s

Fig. 2

Simplified Band Structure

Unintentially-Doped GaAs

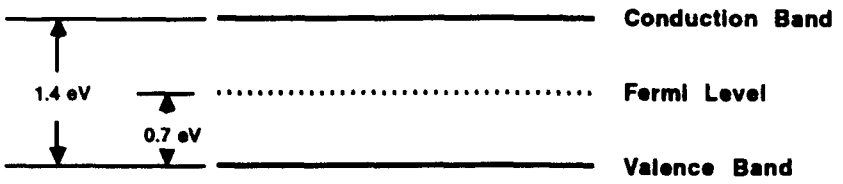

GaAs:As

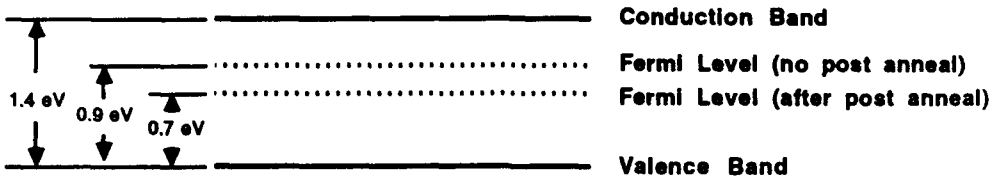

In(0.35)Ga(0.65)As:As

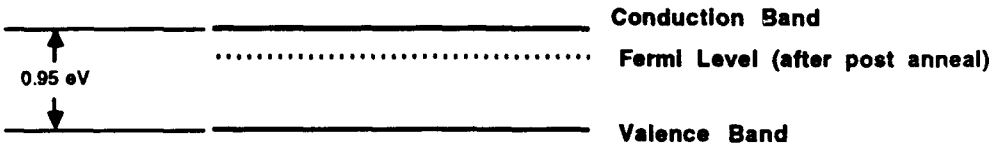

In(0.53)Ga(0.46)As:As

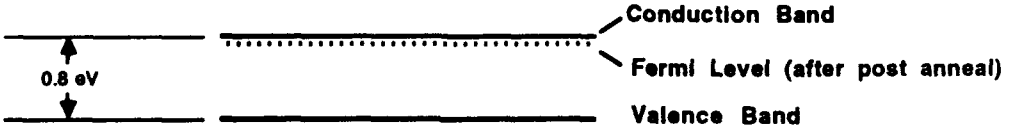

Fig. 3

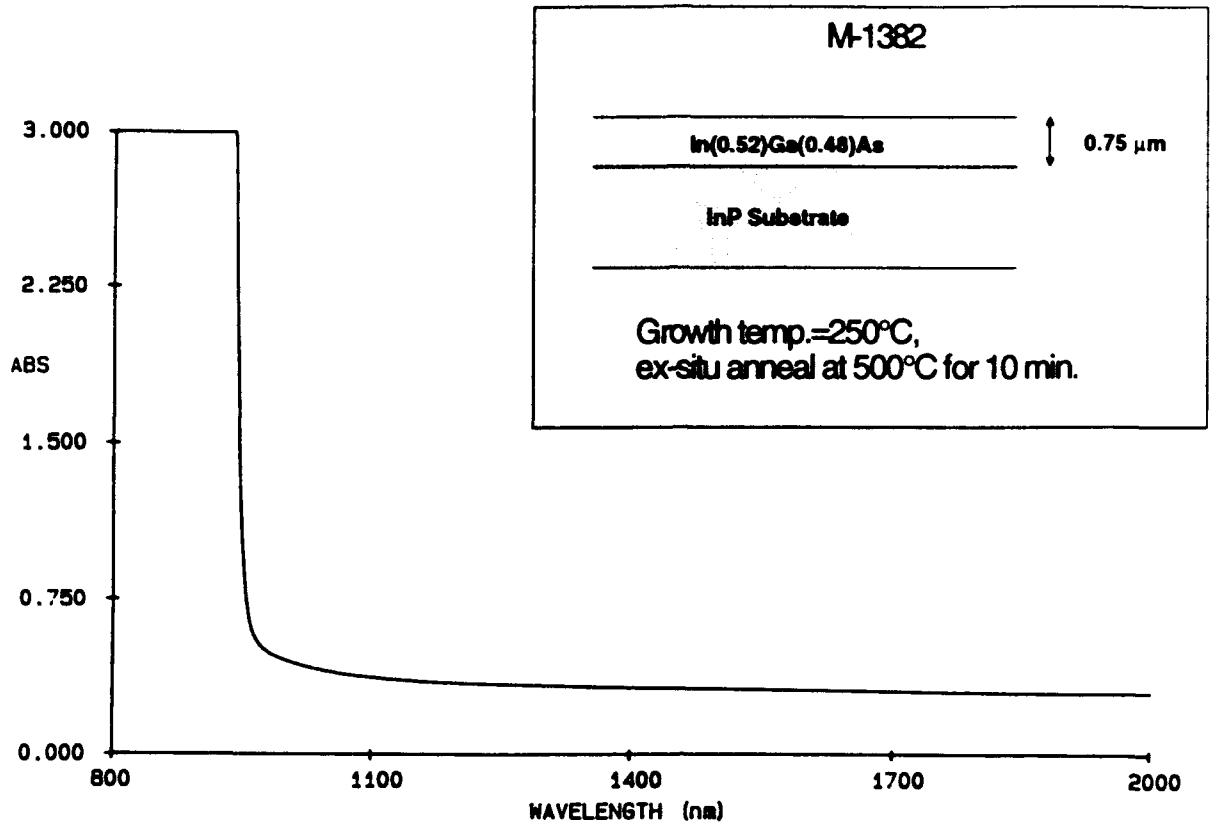
M-1382
In(0.52)Ga(0.48)As
0.75 μm
InP Substrate
Growth temp.=250°C,
ex-situ anneal at 500°C for 10 min.
3.000
2.250
1.500
0.750
0.000
ABS
800
1100
1400
1700
2000
WAVELENGTH (nm)

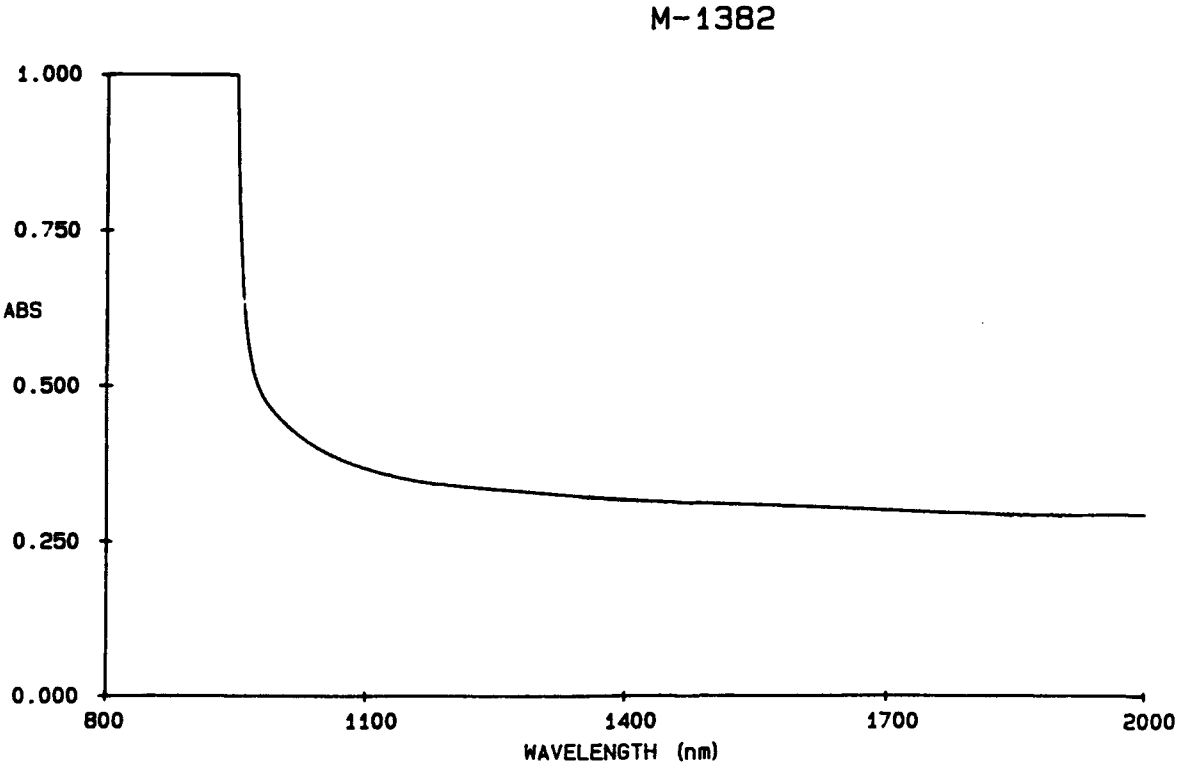
M-1382
1.000
0.750
0.500
0.250
0.000
ABS
800
1100
1400
1700
2000
WAVELENGTH (nm)

Fig. 4

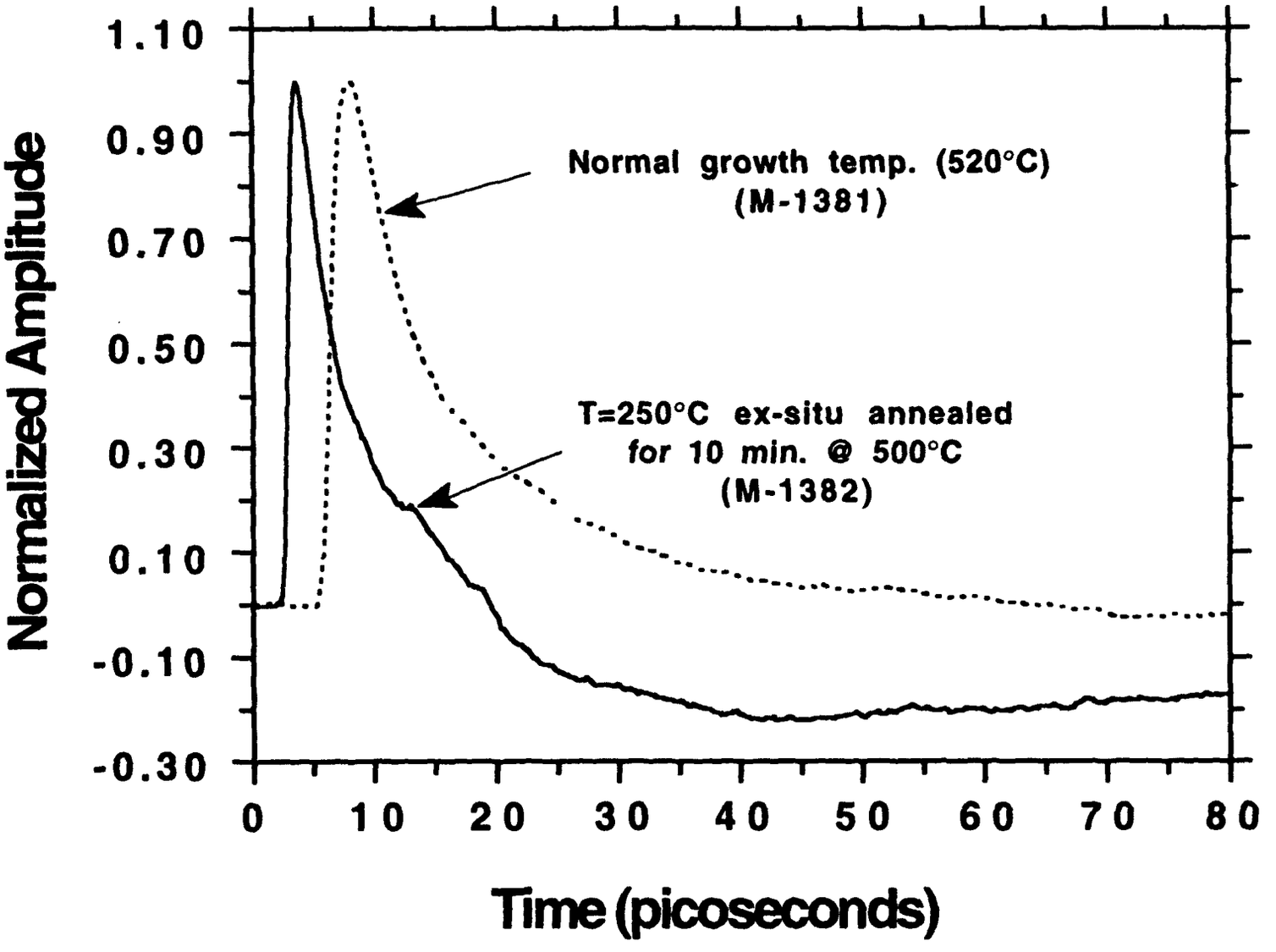
Transient Reflectivity for $In_{0.52}Al_{0.48}As$
Normalized Amplitude
1.10
0.90
0.70
0.50
0.30
0.10
-0.10
-0.30
0
10
20
30
40
50
60
70
80
Time (picoseconds)
Normal growth temp. (520°C)
(M-1381)
T=250°C ex-situ annealed
for 10 min. @ 500°C
(M-1382)

Fig. 5

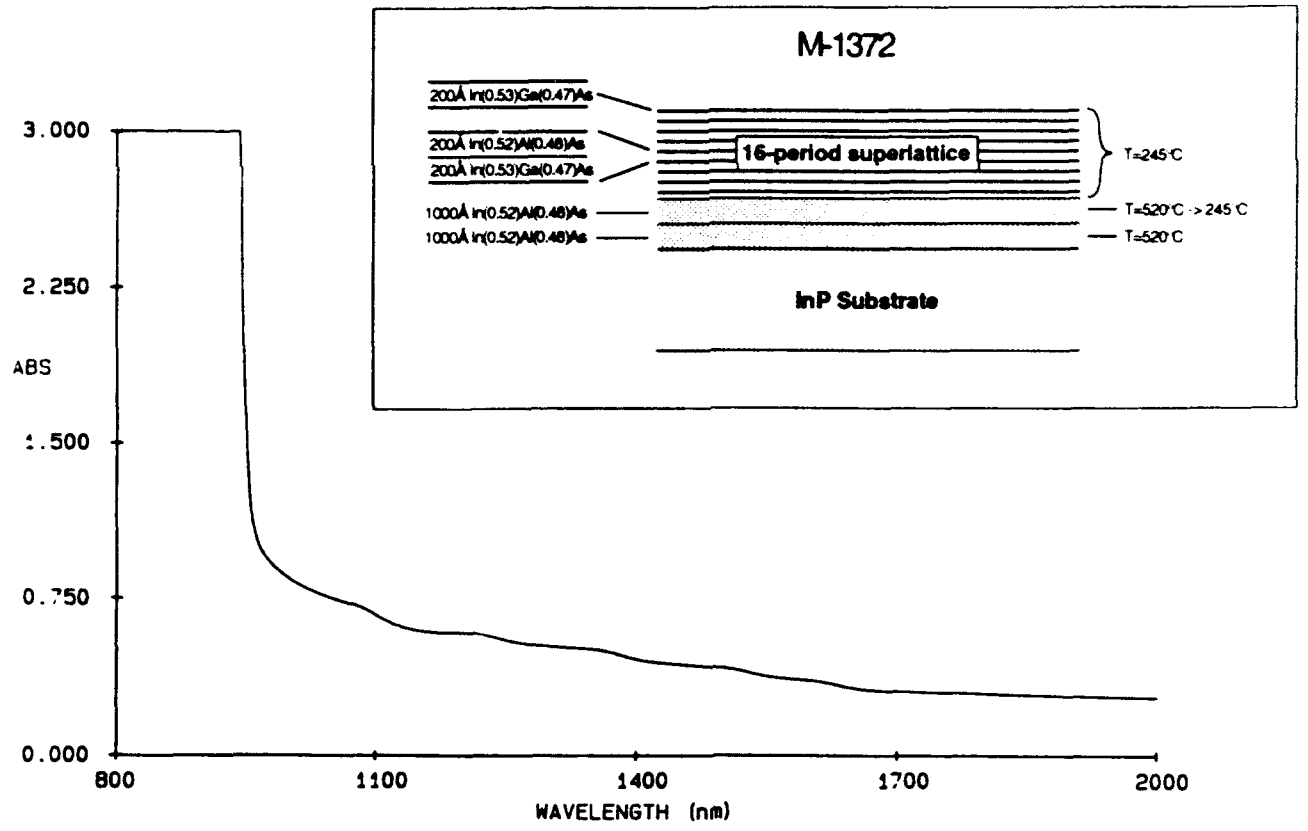
M-1372
200Å In(0.53)Ga(0.47)As
200Å In(0.52)Al(0.48)As
200Å In(0.53)Ga(0.47)As
16-period superlattice
T=245°C
1000Å In(0.52)Al(0.48)As
T=520°C -> 245°C
1000Å In(0.52)Al(0.48)As
T=520°C
InP Substrate
3.000
2.250
ABS
1.500
0.750
0.000
800
1100
1400
1700
2000
WAVELENGTH (nm)

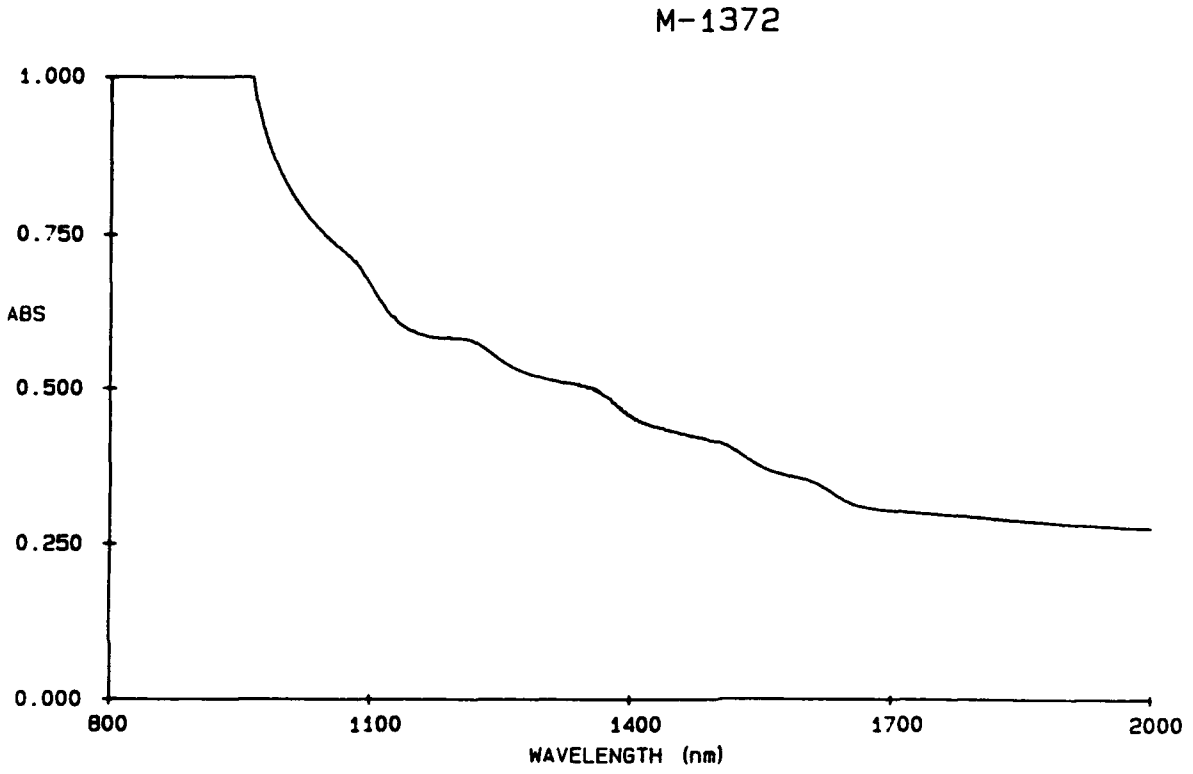
M-1372
1.000
0.750
ABS
0.500
0.250
0.000
800
1100
1400
1700
2000
WAVELENGTH (nm)

Fig. 6

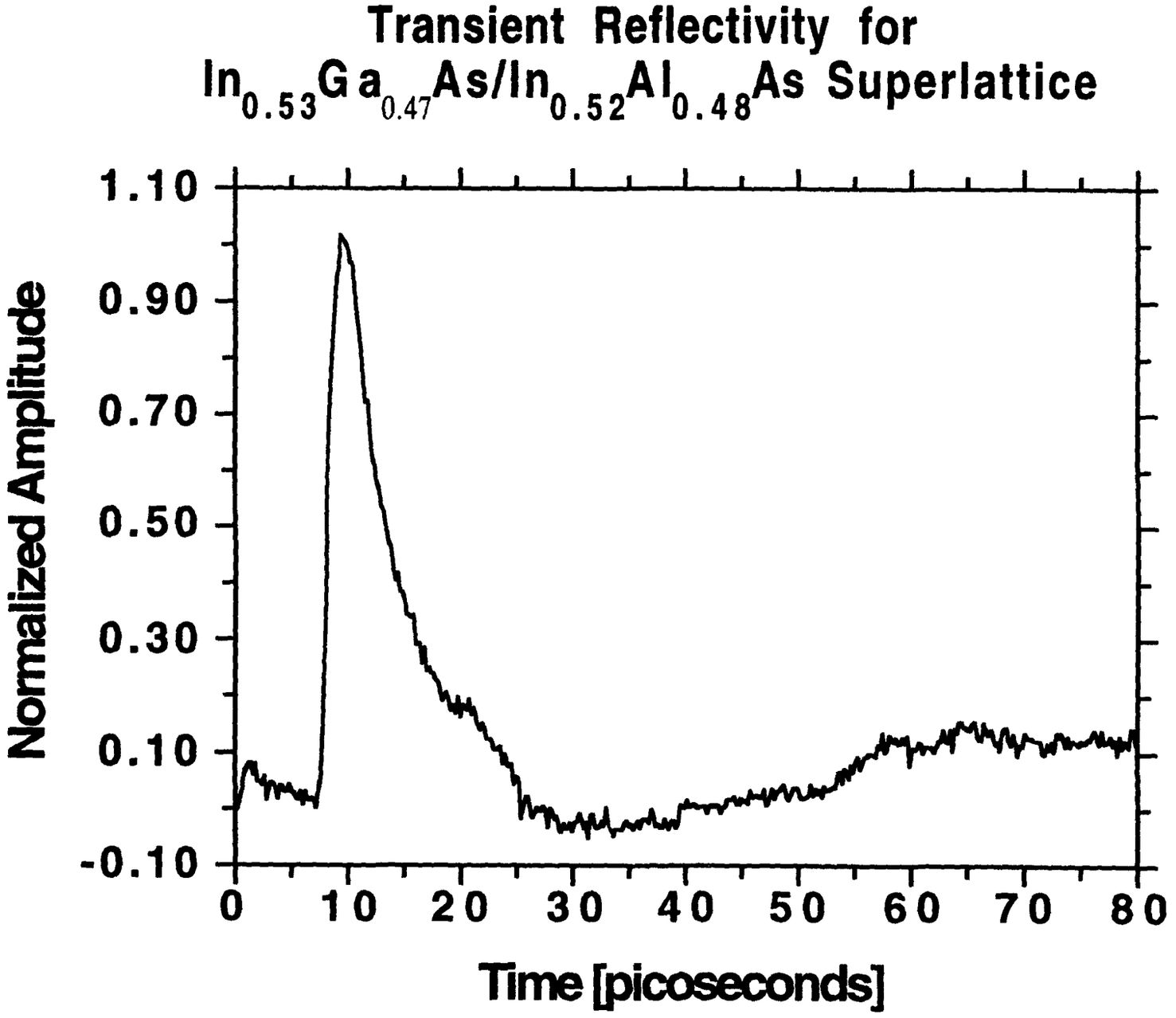
Transient Reflectivity for
In0.53Ga0.47As/In0.52Al0.48As Superlattice
Normalized Amplitude
1.10
0.90
0.70
0.50
0.30
0.10
-0.10
0
10
20
30
40
50
60
70
80
Time [picoseconds]

Fig. 7